# Energetics of Protein Nucleation on Rough Polymeric Surfaces

**Efrem Curcio,*[,†,‡] Valerio Curcio,[§] Gianluca Di Profio,[†,‡] Enrica Fontananova,[†,‡] and Enrico Drioli[†,‡]**

*Department of Chemical Engineering and Materials, University of Calabria, Via P. Bucci, Cubo 44A, 87030 Rende (CS), Italy, Institute on Membrane Technology ITM-CNR, c/o University of Calabria, Via P. Bucci, Cubo 17C, 87030 Rende (CS), Italy, and Liceo Scientifico "T. Lucrezio Caro", Via Vittorio Alfieri 58, 35013 Cittadella (PD), Italy*

*Received: July 9, 2010; Revised Manuscript Received: September 28, 2010*

Metropolis Monte Carlo (MC) algorithm of the two-dimensional Ising model is used to study the heterogeneous nucleation of protein crystals on rough polymeric surfaces. The theoretical findings are compared to those obtained from classical nucleation theory (CNT), and to experimental data from protein model hen egg white lysozyme (HEWL) crystallized on poly(vinylidene fluoride) or PVDF, poly(dimethylsiloxane) or PDMS and Hyflon homemade membranes. The reduction of the activation energy for the nucleation process on polymeric membranes, predicted to occur at increasing surface roughness, results in a nucleation kinetics that is many orders of magnitude faster than in homogeneous phase. In general, MC stochastic dynamics offers the unique opportunity to investigate the effects of collective molecular aggregation at site level on the nucleation rate and, consequently, allows to identify optimal morphological and structural properties of polymeric membranes for a fine control of the crystallization kinetics.

## Introduction

Crystallization is today recognized as a topic of strategic relevance in proteomics because it serves as the basis for X-ray diffraction analysis, the major technique that, together with contemporary NMR spectroscopic methods applied in the physiological conditions of biomacromolecular solutions, is able to yield structural information of proteins at atomic level. Unfortunately, due to the poor aptitude of macromolecules to aggregate in a ordered lattice, crystallization is often referred to as the bottleneck for their three-dimensional structure determination. In this framework, the nucleation of protein crystals on heterogeneous surfaces has emerged in recent years, both theoretically and practically, as one of the most interesting and promising approaches.[1] Crystallization tests carried out on silicon substrates,[2] polymeric films with ionizable groups,[3] glass surfaces made hydrophobic by coating with dimethyldisilazane,[4] Langmuir−Blodgett protein thin films,[5] and microporous hydrophobic polypropylene and poly(vinylidene fluoride) membranes[6,7] are only few examples taken from the recent literature.

According to these studies, the possibility to modulate the geometrical properties (porosity, pore size, roughness, etc.) and physicochemical parameters (i.e., hydrophobic character) of the surfaces, and to operate at lower supersaturation with respect to that requested to activate homogeneous nucleation, enhances the probability to obtain crystals with appropriate size and high structural order using reduced amounts of protein.

Although experimental investigations provide a clear connection between physicochemical−structural properties of the membrane and crystallization kinetics, these findings are not yet supported by a solid theoretical understanding of nucleation phenomena at molecular site level as a premise for a rational strategy of crystal engineering. This research area, still largely underdeveloped, is in most part anchored to the Classical Nucleation Theory developed by Volmer and Weber in 1926.[8] As an alternative approach, Monte Carlo simulation of the Ising model has been used to investigate collective effects occurring in the nucleation of a new phase undergoing to first-order phase transition. 2D Ising model has been successfully applied to study heterogeneous nucleation on square lattice with nearest-neighbor interactions and free boundary conditions.[9] Sear used the same approach to determine the heterogeneous nucleation rate on microscopic impurities, and it was found more than 4 orders of magnitude faster than homogeneous nucleation.[10] Page and Sear investigated the nucleation on the pores, showing that the formation of critical nuclei often proceeds via two steps: nucleation of pore filling and successive nucleation out of pore.[11] As we are specifically interested in investigating the energy of heterogeneous nucleation on rough polymeric membranes, with the aim to demonstrate the sensitivity of crystallization kinetics on the geometrical profile of the surface, we implemented Metropolis Monte Carlo algorithm for studying the Ising energy function of a finite square lattice. The theoretical results are compared to those obtained from classical nucleation theory (CNT), and to experimental data from hen egg white lysozyme (HEWL) crystallization tests grown on poly(vinylidene fluoride) (PVDF), poly(dimethylsiloxane) (PDMS), and Hyflon membrane surfaces.

## Ising Model

We consider here a 2D Ising model on a finite square lattice $\Lambda = \{1...N\}^2$ with spin $\sigma$ in the configuration $\sigma \in \Omega$, with $\Omega = \{-1, +1\}$.

The energy function of the system for spin−spin and spin−field interactions is

* Corresponding author. Tel: +39 0984 496698. Fax: +39 3984 496655. E-mail: e.curcio@unical.it.

† Department of Chemical Engineering and Materials, University of Calabria.

‡ Institute on Membrane Technology ITM-CNR, c/o University of Calabria.

§ Liceo Scientifico "T. Lucrezio Caro".

10.1021/jp106349d © 2010 American Chemical Society
Published on Web 10/12/2010

$$E = -J\sum_{ij}{}'\sigma_i\sigma_j - h\sum_i \sigma_i - J_s\sum_{ij}{}''\sigma_i\sigma_j \quad (1)$$

where $\sigma_{i,j} = \pm 1$ is the state of spin, $J$ is the coupling constant between free spins, $h$ is the external magnetic field, and $J_s$ is the strength of the coupling between a free spin and a fixed spin of the surface. In the right-hand side of eq 1, the first term refers to interactions between free spins, and the single prime on the sum indicates that it is over all nearest-neighbor pairs $ij$ of free spins. The second term accounts for the interactions between free spins and the external magnetic field $h$. The third term is for interactions between the free spins and the fixed spins of the wall, and the double prime on the sum indicates that it is over all nearest-neighbor pairs $ij$ of free and fixed spins.

The surface is formed of a region where spins are fixed to $\sigma_i = +1$, as shown in Figure 1. It is assumed here that $J_s = 0$; that is, the polymeric surface does not preferentially attract either phase; justification arises when considering free energies of surface/spin-up and of surface/spin-down phases identical for a contact angle of 90°, a value not too far from those experimentally measured for polymeric PVDF, Hyflon, and PDMS surfaces.

All the simulations described use a lattice of size $L = 40$ and a coupling constant $J = 0.7\ kT$, where $k$ is the Boltzmann constant, larger than the critical point of the 2D Ising model at $J = 0.44\ kT$;[12] a low external magnetic field $h = 0.05\ kT$ is also included. The parameter $J$ is set in agreement with previous studies.[10,13] However, in order to justify, at a first approximation, its consistency with the physicochemical properties of HEWL, the protein model used in our study, we applied the mathematical expression derived by Onsager for the interfacial tension $\gamma$ between the bulk spin-up and spin-down phases in 2D Ising model with zero external field:[12]

$$\frac{\gamma}{kT} = 2\frac{J}{kT} - \ln\left[\frac{\left(1 + \exp\left(-2\frac{J}{kT}\right)\right)}{\left(1 - \exp\left(-2\frac{J}{kT}\right)\right)}\right] \quad (2)$$

For $J/kT = 0.7$, the predicted value of $\gamma$ is 0.9 $kT$ per site. Assuming that the size of each site corresponds to the molecular diameter of HEWL (~3 nm),[14] we calculated a surface tension of 0.5 mN/m, not so far from the value of 1 mN/m that is the HEWL solid−liquid interface tension experimentally measured by Krishnan et al.[15] It is worth specifying that eq 2 is strictly valid for interface of the infinite length with ⟨10⟩ mean running direction; on the other hand, our system is characterized by an interface of finite length, and its anisotropy would require a interface tension value with ⟨11⟩ mean running direction. Despite this approximation, the coherence between the theoretical prediction of $\gamma$ and its experimental value can be considered satisfactory and, consequently, the choice of $J$ appropriate.

Simulation makes use of the standard Metropolis Monte Carlo method for spin flipping: flip is always accepted if it lowers the energy or, otherwise, accepted with probability of $\exp(-\Delta E/kT)$, where $\Delta E$ is the energy difference due to spin flip and $k$ is the Boltzmann constant.[16]

The forward flux sampling (FFS) algorithm recently proposed by Allen and co-workers was used to manage the rare nucleation events.[17,18] To check the correctness of the implemented FFS algorithm, preliminary simulations were performed under the same conditions ($J/kT = 0.65$, $h/kT = 0.05$, $L = 45$) investigated by Sear[10] and Allen et al.[13] The homogeneous nucleation rate per site and per cycle was of $(3.2 \pm 0.2) \times 10^{-13}$, in good agreement with literature results. For $L = 40$, the nucleation rate was $(3.1 \pm 0.2) \times 10^{-13}$, thus ensuring that our box size was sufficient to make computed events substantially independent of $L$. However, heterogeneous nucleation rates on rough surfaces were high enough ($>9 \times 10^{-7}$) to be evaluated also by direct simulation.

### Classical Nucleation Theory (CNT)

CNT predicts that, for nucleation taking place on a ideally smooth and planar surface, the ratio $\phi$ of the activation energy for heterogeneous nucleation $\Delta E^*_{het}$ to the energy threshold for homogeneous nucleation $\Delta E^*_{hom}$ depends on the contact angle $\theta$ according to the following equation:[19]

$$\frac{\Delta E^*_{het}}{\Delta E^*_{hom}} = \phi = \frac{1}{4}(1 - \cos\theta)^2(2 + \cos\theta) \quad (3)$$

The activation (Gibbs' free) energy directly affects the nucleation rate $N_{CNT}$

$$N_{CNT} = \nu \exp\left(-\frac{\phi\Delta E^*_{hom}}{R_g T}\right) \quad (4a)$$

with

$$\Delta E^*_{hom} = \frac{16}{3}\pi\gamma_l\left(\frac{v}{\Delta\mu}\right)^2 \quad (4b)$$

In eqs 4a and 4b, $\nu$ is the collision factor, $R_g$ the gas constant, $\gamma_l$ the nucleus−liquid interfacial tension, $v$ the molar volume, and $\Delta\mu$ the chemical potential gradient.

For nucleation occurring on a rough surface, the energy $\Delta E_{het,rough}$ can be calculated as sum of the bulk and surface terms

$$\Delta E_{het,rough} = \left(-\frac{\Delta\mu}{v}\right)V + \gamma_l A_l - (\gamma_s - \gamma_i)A_{sl} \quad (5)$$

where $V$ is the nucleus volume, $A_l$ the surface area of the nucleus spherical cap, and $A_{sl}$ the nucleus−solid interfacial area; surface tensions $\gamma_l$, $\gamma_i$, and $\gamma_s$ refer to nucleus−liquid, nucleus−surface, and liquid−surface, respectively.

From simple geometric and trigonometric procedures based on Figure 2

$$V = \frac{\pi}{3}R^3(1 - \cos\theta)^2(2 + \cos\theta) + \pi R^2 h \sin^2\theta - \frac{\pi}{3}ms^2h \quad (6a)$$

$$A_l = 2\pi R^2(1 - \cos\theta) \quad (6b)$$

$$A_{sl} = \pi R^2 \sin^2\theta - m\pi s^2 + ms\sqrt{s^2 + h^2} \quad (6c)$$

where $m$ is the number of asperities on the surface.

The wetting behavior of rough surfaces is usually described by the Wenzel equation

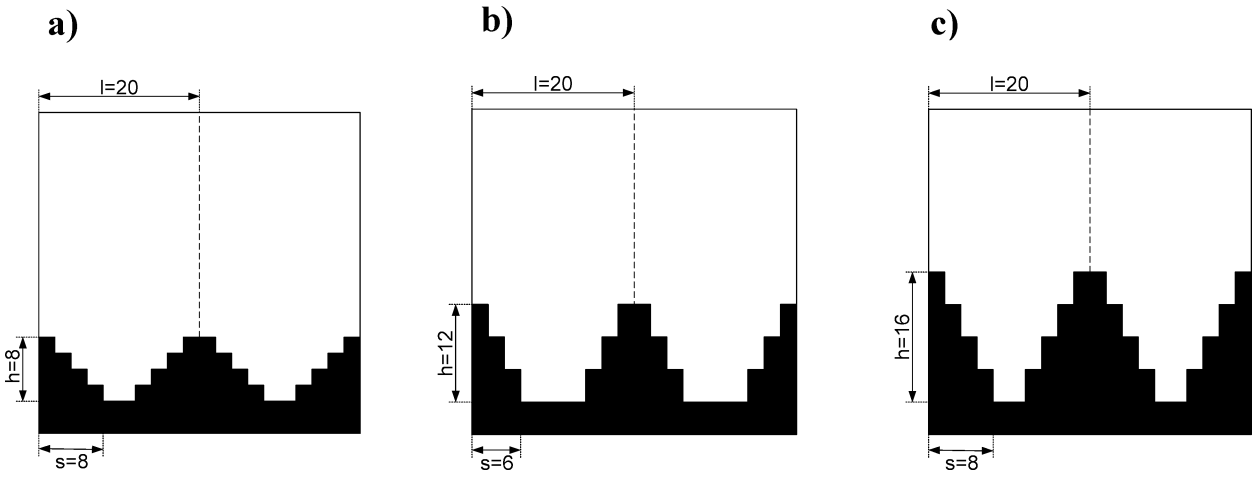


**Figure 1.** Ising lattices of 40 × 40 sites. Black sites, identifying surface asperities, with fixed spins up $\sigma_i = +1$; the bulk (white sites) is in the spin-down phase $\sigma = -1$. The three initial configurations correspond to different surface roughness coefficients: (a) $r = 1.20$; (b) $r = 1.33$; (c) $r = 1.59$.

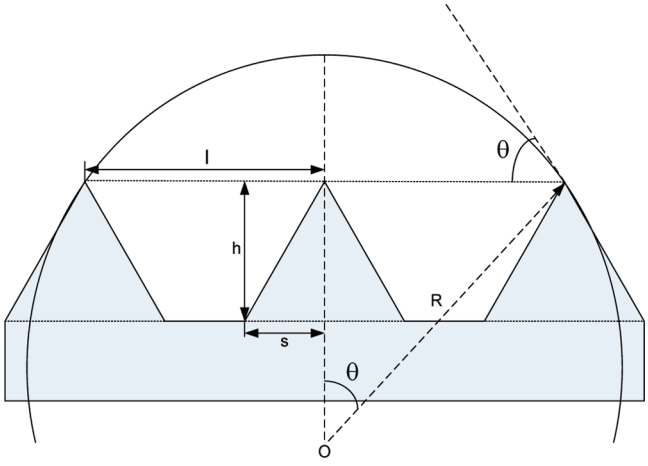


**Figure 2.** Geometry of a sphere cap nucleus on a rough surface. Symbols *h*, *s*, and *l* are related to Figure 1.

$$(\gamma_s - \gamma_i) = \frac{1}{r}\gamma_l \cos\theta \tag{7}$$

where $r$ is the Wenzel roughness factor, defined as the ratio of corrugated surface to the projected area ($r > 1$). Referring to Figure 2, and assuming that asperities on the membrane surface have a conical shape, the roughness factor $r$ can be evaluated as

$$r = \frac{(\pi l^2 - m\pi s^2) + m\pi s\sqrt{h^2 + s^2}}{\pi l^2} \tag{8}$$

where $h$ is the asperity height, $l$ is the distance between two consecutive asperity peeks, and $s$ and $m$ are the half-base length and the number of cones, respectively.

The maximum value of the activation energy, $\Delta E^*_{het,rough}$, is calculated by differentiating eq 5 and imposing

$$\partial \Delta E_{het}/\partial R = 0 \tag{9}$$

Equations were computed in Matlab R2007b (MathWorks Inc.).

**TABLE 1: Relevant Membrane Characteristics**

| membrane type | water contact angle (deg) | protein solution contact angle (deg) | rms roughness (nm) | Wenzel roughness factor from AFM height profile |
|---|---|---|---|---|
| Hyflon | 108 ± 0.75 | 101 ± 4.3 | 6 | 1.10 |
| PVDF | 87.4 ± 2.5 | 87.0 ± 2.0 | 22 | 1.24 |
| PDMS | 128 ± 0.50 | 105 ± 3.8 | 45 | 1.52 |

## Materials and Methods

PVDF polymeric membranes were prepared from solutions of 20 wt % poly(vinylidene fluoride) homopolymer (Elf Autochem) and *N*,*N*-dimethylacetamide (Sigma-Aldrich) by non-solvent-induced phase inversion method.[20] PDMS membranes were prepared from solutions of 25 wt % poly(dimethylsiloxane), synthesized from prepolymer RTV 615 A and cross-linker RTV 615 B mixed with ratio 10:1, both provided by General Electric, and dichloromethane (Sigma-Aldrich) by solvent-evaporation phase inversion method.[21] Hyflon membranes were prepared from solutions of 10 wt % Hyflon AD 60X (copolymer of tetrafluoroethylene and 2,2,4-trifluoro-5-trifluoromethoxy-1,3-dioxole) and Galden HT55, both supplied by Solvay Solexis, by solvent-evaporation phase inversion method.

Static contact angles were measured by sessile drop method using CAM 200 contact angle meter (KSV Instruments Ltd., Helsinki, Finland) equipped with microsyringe, automatic dispenser, and software for image acquisition and processing. Topography and root-mean-square (rms) roughness of the membrane surfaces were investigated by atomic force microscopy (AFM; Nanoscope III Digital Instruments, VEECO Metrology Group) in a tapping mode AFM imaging across 10 × 10 $\mu m^2$ of the sample surface at a rate of 1.0 Hz. The physicochemical membrane properties of relevance for our study are summarized in Table 1.

For crystallization tests, carried out at 5 °C, hen egg white lysozyme (HEWL) (Sigma-Aldrich), lyophilized and three times recrystallized, was used without additional purification. The protein was dissolved in 0.05 M NaAc buffer at pH 4.5; a precipitant solution was also prepared by dissolving NaCl (Sigma-Aldrich) in the buffer. Both solutions were filtered and mixed 1:1 to give a final NaCl concentration of 2 wt % a final protein concentration of 40 mg/mL.[7] Crystals were observed by optical microscope Axiovert 25 (Zeiss) equipped with a video

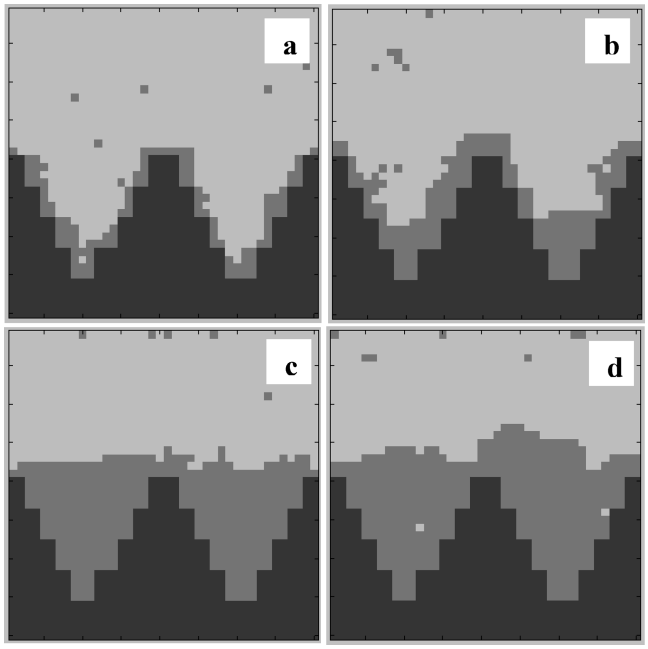


**Figure 3.** A sequence of snapshots of the 40 × 40 lattice box emulating a surface with roughness coefficient of 1.59 ($J/kT = 0.7$, $h/kT = 0.05$) at (a) $2.0 \times 10^3$ cycles*sites; (b) $1.8 \times 10^4$ cycles*sites; (c) $1.9 \times 10^4$ cycles*sites; (d) $2.0 \times 10^4$ cycles*sites. The fixed spins are black ($\sigma = +1$), up spins are gray, and down spins are light gray.

camera JVC, TK-C1480B, scored by number and size at intervals of 12 h.

## Results and Discussion

A time sequence of computer simulation snapshots of the 40 × 40 Ising lattice corresponding to a surface with roughness coefficient of 1.59 is reported in Figure 3. According to Figure 3a, the rough profile of the surface offers preferential sites to spin flipping from down to up phase, whereas in the bulk of the system isolated up spins appear not susceptible of aggregation in clusters. A complete flipping to spin-up phase of sites adjacent to the membrane surface is observed at $2.0 \times 10^3$ cycles*sites. The system remains almost stable in this configuration for several cycles, until a rapid coalescence of up spins occurs at the valley bottom (Figure 3b). This is coherent with the existence of a activation barrier for valleys filling that occurs at $\sim 1.9 \times 10^4$ cycles*sites (Figure 3c); this value can be interpreted as the induction time $\tau_{Ising}$ required by the system to leave the metastable state. In the nucleation regime, only one cluster grows and engulfs the whole lattice, and the induction time is inversely proportional to the nucleation rate $N_{Ising}$ ($N_{Ising} = \tau_{Ising}^{-1}$); therefore, for $r = 1.59$, $N_{Ising} = 5.2 \times 10^{-5}$ #/cycle*site. Systems with lower roughness coefficient were characterized by shorter induction times: $4.8 \times 10^4$ cycles*sites for $r = 1.33$, and $1.1 \times 10^6$ cycles*sites for $r = 1.20$.

Nucleation kinetics has been investigated by evaluating the size of the critical cluster $n^*$ and the corresponding energy barrier $\Delta E^*$ to nucleation. Homogeneous nucleation was simulated by setting up a cluster of $n$ spins ($50 \le n \le 350$) with $\sigma = +1$ in the middle of the 2D lattice surrounded by a sea of spins with $\sigma = -1$; heterogeneous nucleation on the rough polymeric membrane was simulated by setting up a cluster of $n$ spins ($50 \le n \le 350$) with $\sigma = +1$ placed at the valley bottom of the surface profile ($\sigma = +1$) and all remaining spins at $\sigma = -1$. Then, by observing the evolution stories of many individual clusters, we define $n^*$ as the number of up spins of that cluster

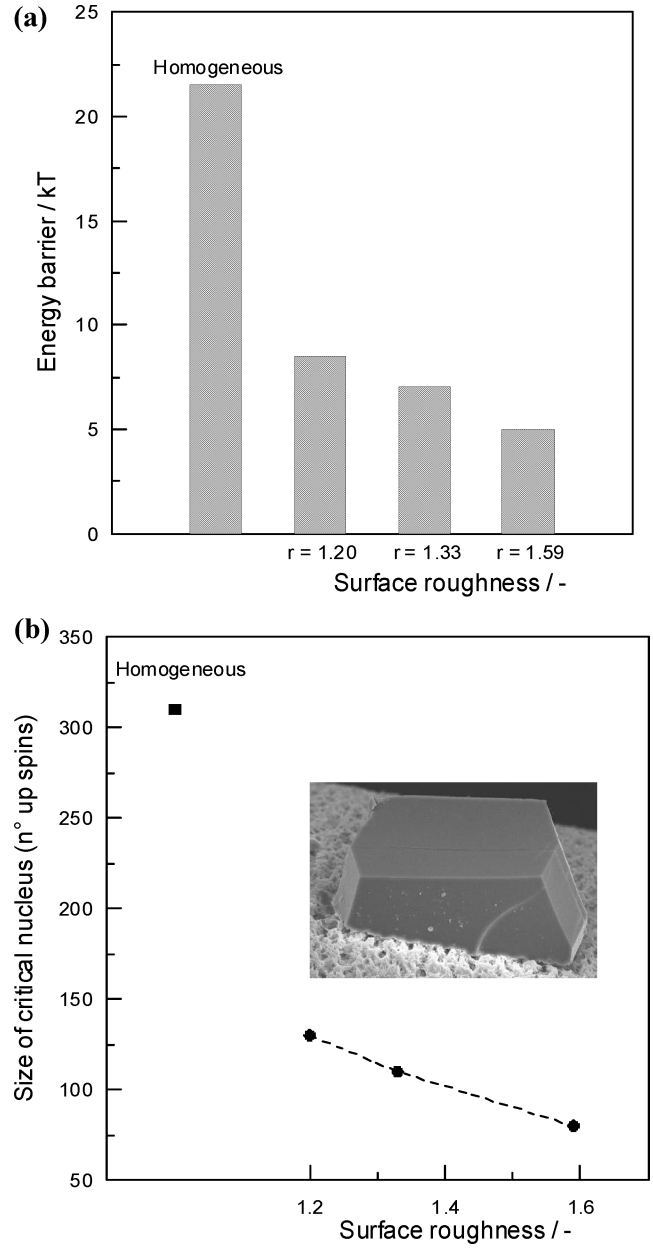


**Figure 4.** Parameters of the critical cluster in homogeneous phase and as a function of surface roughness: (a) energy barrier, $\Delta E^*/kT$; (b) size, $n^*$. Inset is a tetragonal HEWL crystal nucleated on the rough surface of a polymeric membrane.

having 50 ± 5% probability to growth or decay in 100 runs (each run consisting of $10^5$ steps) of Monte Carlo stochastic dynamics.[22]

Theoretical results reported in Figure 4a show that, for $J = 0.7$ $kT$ and $h = 0.05$ $kT$, the value of energy barrier for homogeneous nucleation is $\sim 21.5$ $kT$; this is in good agreement with data of Allen and colleagues who reported a $\Delta E^*$ of $\sim 22$ $kT$ at $J = 0.65$ kT and $h = 0.05$ $kT$.[13] These findings confirm that nucleation proceeds at low supersaturation, resulting in a single growing large cluster of up spins. In the study of Brendel et al., measurements of the distribution of cluster sizes in a 64 × 64 2D Ising lattice at $J/kT = 0.53$ and $h/kT = 0.08$ resulted in a maximum value of free energy of $\sim 28$ $kT$.[23]

Our result is also in nice agreement with the value of 24.9 $kT$ calculated by using the Becker−Döring expression for the free energy $E$[24]

$$E(n) \approx E_0 + 2\gamma\sqrt{\pi n} - 2hn \qquad (10)$$

where the cluster size $n$ is replaced by the critical size $n^* = 310$ (as from Figure 4b), the constant $E_0$ is set to 0, $\gamma \sim 0.9\ kT$ is the surface tension as evaluated by the Onsager expression (eq 2) although strictly valid under zero external field, and $h = 0.05\ kT$.

As expected, both size and free energy of the critical cluster are reduced in heterogeneous phase in the presence of a rough surface: in this case, probability and frequency of nucleation events are enhanced at higher roughness coefficient. In particular, the energy barrier is decreased by 60% (from 21.5 to 8.5 $kT$) for nuclei growing on a surface with $r = 1.2$; the critical size is consequently reduced from 310 to 130 up spins. A further decrease of both $n^*$ and $\Delta E^*$ was observed at increasing $r$, and the lowest energy barrier ($\sim$5 $kT$) and cluster size (80 up spins) was found for the most rough simulated profile ($r = 1.59$).

Simulation results of the 2D Ising model were checked against CNT predictions. Figure 5 illustrates the ratio between the energy barrier for homogeneous nucleation and for heterogeneous nucleation on rough surfaces, as obtained from eq 5 followed by maximization condition expressed by eq 9. Values for parameters $m$, $s$, $h$, and $l$ have been assigned in agreement with the geometric characteristics of the 2D Ising lattices considered, as illustrated in Figure 1. The $\Delta E^*_{het,rough}/\Delta E^*_{hom}$ increases with the contact angle and, for the limiting value of $\theta = 180°$, the curves converge to 1 (nucleation in homogeneous phase). For a perfectly smooth surface, characterized by a roughness coefficient $r = 1$, the ratio is expressed by eq 3; in particular, for $\theta = 90°$ (the reference value for our Monte Carlo simulations) $\Delta E^*_{het,rough}/\Delta E^*_{hom} = 0.5$. CNT predicts that the energy barrier is progressively decreased at increasing surface roughness, thus resulting in a exponentially faster nucleation process.

The experimental activity of many authors confirms these theoretical findings. The work of Gunn showed that the nucleation rate of calcium sulfate dihydrate is increased by the roughness of heated stainless steel surfaces where $CaSO_4 \cdot 2H_2O$ is deposited.[25] Falini et al. suggested that an increase of the wettability and of the roughness of mica surfaces tested in protein crystallization promotes nonspecific and local interactions that contribute to the enhance nucleation rate.[26] The influence of surface topography of copper (Cu) sheet on the heterogeneous nucleation of isotactic polypropylene (iPP) at the iPP/Cu interface has been investigated by Lin et al.[27] HEWL crystallization tests carried out by Liu et al. on poly(L-glutamic acid), poly(2-hydroxyethyl methacrylate), and (3-aminopropyl)-triethoxysilane surfaces demonstrated that the specific topography significantly affects the nucleation rate.[28]

Figure 6 compares the results of Ising model and CNT predictions at $\theta = 90°$ and different roughness coefficient. The agreement is satisfactory, although the Ising model seems to underestimate the reduction of energy barrier to heterogeneous nucleation; for moderately rough surfaces ($r < 1.25$), the difference between Ising model and CNT results is lower than 10%, whereas deviation exceeds 20% for $r > 1.55$. These observations are coherent with findings of Acharyya and Stauffer who claimed a substantial agreement of Ising model with CNT if surface tension $\gamma$ is increased $\sim$4/3 times the macroscopic value.[29]

A qualitative comparison between theoretical and experimental nucleation rate was also performed. In fact, protein crystallization is a rather complex process, not only influenced by the physicochemical and structural characteristics of the surface: electrostatic interactions between protein molecules and polymeric membranes, and preferential adsorption of macromolecules at hydrophobic surfaces rather than hydrophilic ones, significantly affect the heterogeneous nucleation kinetics. Moreover, Ising model permits to evaluate the nucleation rate beyond a unpredictable proportionality factor, and it can be expressed in the unit of number of critical nuclei formed per Monte Carlo step and lattice site. As seen in Figure 7, the values of $N_{Ising}$ span over 2 orders of magnitude from $9.1 \times 10^{-7}$ #/cycle*site at low roughness ($r = 1.2$) to $5.2 \times 10^{-5}$ #/cycle*site at $r = 1.59$. As a rough comparison with literature data, Sear obtained a nucleation rate on a impurity of 6 spins in the order of $10^{-5}$ #/cycle*site, compared to a homogeneous nucleation rate of $\sim 10^{-13}$ #/cycle*site.[10]

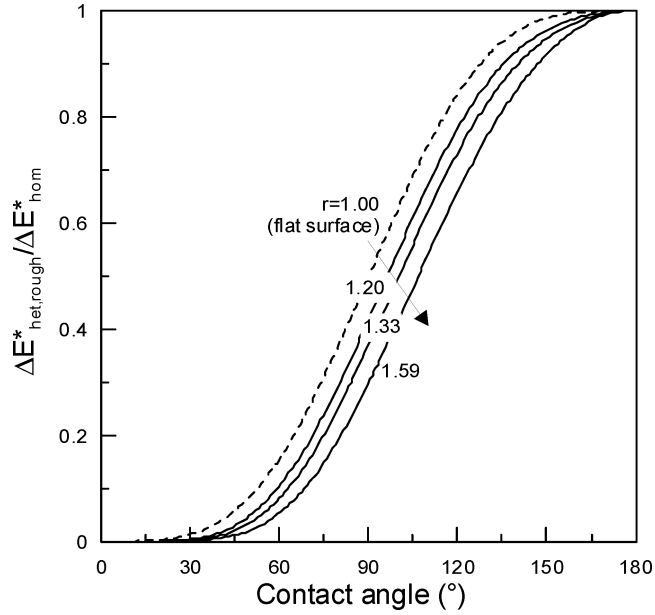


**Figure 5.** Ratio of the activation energy for homogeneous and heterogeneous nucleation processes as a function of the contact angle. Curves are derived for different surface roughness.

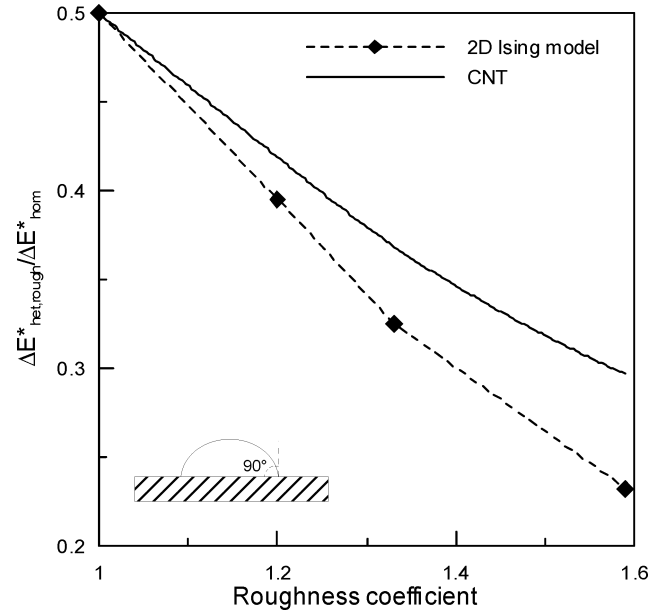


**Figure 6.** Comparison between Ising model and CNT results for $\Delta E^*_{het,rough}/\Delta E^*_{hom}$ as a function of roughness coefficient. Data refers to contact angle of 90°.

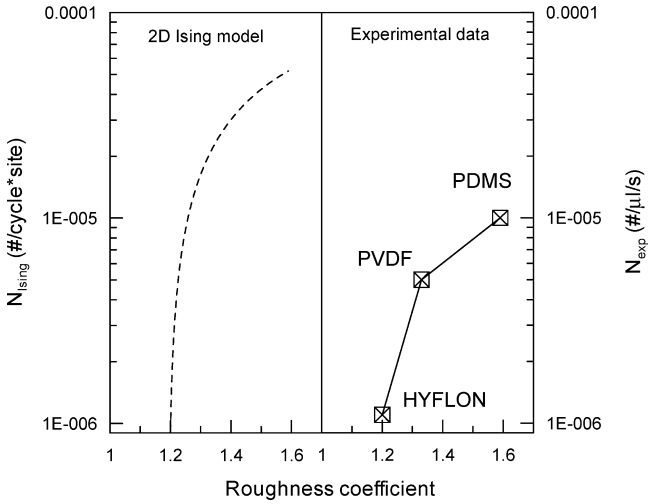


**Figure 7.** Theoretical and experimental nucleation rate as a function of the roughness coefficient.

The increasing trend of $N_{Ising}$ with $r$ is experimentally confirmed by crystallization tests on lysozyme. The measured HEWL nucleation rate using PVDF membrane, characterized by a roughness coefficient of 1.25, is $5 \times 10^{-6}$ #/$\mu$L s; this is 5 times higher than the value measured on Hyflon membranes ($r = 1.1$). The faster nucleation process, occurring with rate of $1 \times 10^{-5}$ #/$\mu$L s, has been detected on PDMS membranes ($r = 1.5$). Induction times, reduced for higher nucleation rates, ranged between 1 and 3 h.

## Conclusions

In this work, 2D Ising model was implemented with the aim to demonstrate the sensitivity of the crystallization kinetics to the roughness of polymeric surfaces used as substrate for heterogeneous nucleation. Our simulation results, expressed in terms of energy barrier to nucleation and size of critical cluster, were consistent with theoretical predictions of classical nucleation theory. Despite its simplicity, Metropolis Monte Carlo simulation algorithm of the Ising model represents a complementary and realistic tool for understanding nucleation phenomena at molecular site level, and for describing the process of early cluster aggregation in terms of discrete spin flipping. Therefore, Monte Carlo stochastic dynamics offers a valuable opportunity to investigate the effect of the geometrical profile of a surface on the heterogeneous nucleation rate and might contribute, in perspective, to a better control of the crystallization kinetics of proteins, biomolecules, and polymorphs.[30]

## References and Notes

(1) Saridakis, E.; Chayen, N. E. *Trends Biotechnol.* **2009**, *27*, 99–106.
(2) Sanjoh, A.; Tsukihara, T.; Gorti, S. *J. Cryst. Growth* **2001**, *232*, 618–628.
(3) Fermani, S.; Falini, G.; Minnucci, M.; Ripamonti, A. *J. Cryst. Growth* **2001**, *224*, 327–334.
(4) Nanev, C. N. *Cryst. Growth Des.* **2007**, *7*, 1533–1540.
(5) Pechkova, E.; Nicolini, C. *J. Cell. Biochem.* **2004**, *91*, 1010–1020.
(6) Curcio, E.; Di Profio, G.; Drioli, E. *J. Cryst. Growth* **2003**, *247*, 166–176.
(7) Curcio, E.; Fontananova, E.; Di Profio, G.; Drioli, E. *J. Phys. Chem. B* **2006**, *110*, 12438–12445.
(8) Volmer, M.; Weber, A. *Z. Phys. Chem.* **1926**, *119*, 277–301.
(9) Cirillo, E. N. M.; Lebowitz, J. L. *J. Stat. Phys.* **1998**, *90*, 211–226.
(10) Sear, R. P. *J. Phys. Chem. B* **2006**, *110*, 4985–4989.
(11) Page, A. J.; Sear, R. P. *Phys. Rev. Let.* **2006**, *97*, 065701.
(12) Onsager, L. *Phys. Rev.* **1944**, *65*, 117–149.
(13) Allen, R. J.; Valeriani, C.; Tanase-Nicola, S.; ten Wolde, P. R.; Frenkel, D. *J. Chem. Phys.* **2008**, *129*, 134704.
(14) Kisler, J. M.; Stevens, G. W.; O'Connor, A. J. *Mater. Phys. Mech.* **2001**, *4*, 89–93.
(15) Krishnan, C. A.; Maheshwari, R.; Dhathathreyan, A. *Chem. Phys. Lett.* **2006**, *417*, 128–131.
(16) Chandler, D. *Introduction to modern statistical mechanics*; Oxford University Press: New York, 1987.
(17) Allen, R. J.; Frenkel, D.; ten Wolde, P. R. *J. Chem. Phys.* **2006**, *124*, 194111.
(18) Allen, R. J.; Frenkel, D.; ten Wolde, P. R. *J. Chem. Phys.* **2006**, *124*, 024102.
(19) Vehkamaki, H. *Classical Nucleation Theory in Multicomponent Systems*; Springer-Verlag: Berlin, 2006.
(20) Fontananova, E.; Jansen, J. C.; Cristiano, A.; Curcio, E.; Drioli, E. *Desalination* **2006**, *192*, 190–197.
(21) Fontananova, E.; Di Profio, G.; Curcio, E.; Giorno, L.; Drioli, E. *J. Inclusion Phenom. Macrocyclic Chem.* **2007**, *57*, 537–543.
(22) Vehkamaki, H.; Ford, I. *J. Phys. Rev. E* **1999**, *59*, 6483–6488.
(23) Brendel, K.; Barkema, G. T.; van Beijeren, H. *Phys. Rev. E* **2005**, *71*, 031601.
(24) Duncan, D. B.; Soheili, A. R. *Appl. Numer. Math.* **2001**, *37*, 1–29.
(25) Gunn, D. J. *J. Cryst. Growth* **1980**, *50*, 533–537.
(26) Falini, G.; Fermani, S.; Conforti, G.; Ripamonti, A. *Acta Crystallogr. D Biol. Crystallogr.* **2002**, *58*, 1649–1652.
(27) Lin, C. W.; Ding, S. Y.; Hwang, Y. W. *J. Mater. Sci.* **2001**, *36*, 4943–4948.
(28) Liu, Y. X.; Wang, X. J.; Lu, J.; Ching, C. B. *J. Phys. Chem. B* **2007**, *111*, 13971–13978.
(29) Acharyya, M.; Stauffer, D. *Eur. Phys. J. B* **1998**, *5*, 571–575.
(30) Llinas, A.; Goodman, J. M. *Drug Discovery Today* **2008**, *13*, 198–210.

JP106349D